PAPER

Mechanisms underlying activation of retinal bipolar cells through targeted electrical stimulation: a computational study

To cite this article: Javad Paknahad et al 2021 J. Neural Eng. 18 066034

View the article online for updates and enhancements.

You may also like

- The impact of calcium current reversal on neurotransmitter release in the electrically stimulated retina Paul Werginz and Frank Rattay

- Young, Blue, and Isolated Stellar Systems in the Virgo Cluster. II. A New Class of

Stellar System
Michael G. Jones, David J. Sand, Michele Bellazzini et al.

- Dynamics and steady states of a tracer particle in a confined critical fluid Markus Gross

Journal of Neural Engineering



10 July 2021

REVISED

24 November 2021

ACCEPTED FOR PUBLICATION 26 November 2021

15 December 2021

PAPER

Mechanisms underlying activation of retinal bipolar cells through targeted electrical stimulation: a computational study

Javad Paknahad^{1,2,*}, Pragya Kosta², Jean-Marie C Bouteiller³, Mark S Humayun^{3,4} and Gianluca Lazzi1,2,3,4

- Department of Electrical and Computer Engineering, University of Southern California, Los Angeles, CA, United States of America
- Institute for Technology and Medical Systems (ITEMS), Keck School of Medicine, University of Southern California, Los Angeles, CA,
- Department of Biomedical Engineering, University of Southern California, Los Angeles, CA, United States of America
- Department of Ophthalmology, University of Southern California, Los Angeles, CA, United States of America
- Author to whom any correspondence should be addressed.

E-mail: paknahad@usc.edu

Keywords: computational modeling, epiretinal prostheses, retinal bipolar cells, network-mediated response of RGCs

Abstract

Objective. Retinal implants have been developed to electrically stimulate healthy retinal neurons in the progressively degenerated retina. Several stimulation approaches have been proposed to improve the visual percept induced in patients with retinal prostheses. We introduce a computational model capable of simulating the effects of electrical stimulation on retinal neurons. Leveraging this computational platform, we delve into the underlying mechanisms influencing the sensitivity of retinal neurons' response to various stimulus waveforms. Approach. We implemented a model of spiking bipolar cells (BCs) in the magnocellular pathway of the primate retina, diffuse BC subtypes (DB4), and utilized our multiscale admittance method (AM)-NEURON computational platform to characterize the response of BCs to epiretinal electrical stimulation with monophasic, symmetric, and asymmetric biphasic pulses. Main results. Our investigations yielded four notable results: (a) the latency of BCs increases as stimulation pulse duration lengthens; conversely, this latency decreases as the current amplitude increases. (b) Stimulation with a long anodic-first symmetric biphasic pulse (duration > 8 ms) results in a significant decrease in spiking threshold compared to stimulation with similar cathodic-first pulses (from 98.2 to 57.5 μ A). (c) The hyperpolarization-activated cyclic nucleotide-gated channel was a prominent contributor to the reduced threshold of BCs in response to long anodic-first stimulus pulses. (d) Finally, extending the study to asymmetric waveforms, our results predict a lower BCs threshold using asymmetric long anodic-first pulses compared to that of asymmetric short cathodic-first stimulation. Significance. This study predicts the effects of several stimulation parameters on spiking BCs response to electrical stimulation. Of importance, our findings shed light on mechanisms underlying the experimental observations from the literature, thus highlighting the capability of the methodology to predict and guide the development of electrical stimulation protocols to generate a desired biological response, thereby constituting an ideal testbed for the development of electroceutical devices.

1. Introduction

Diseases such as retinitis pigmentosa (RP) and agerelated macular degeneration (AMD) start with degeneration of photoreceptors, which are located at the outermost layer of the retina, and eventually damage the innermost layer of the retina, consisting of retinal ganglion cells (RGCs). Retinal and

cortical implant based visual prosthetic systems have had a significant impact on the life of patients who have been blinded for decades due to these diseases by providing useful partial sight that improves mobility [1-6]. Epiretinal implants aim at electrically stimulating the surviving retinal neurons, such as RGCs, which remain largely viable compared to outermost and intermediate neurons at the late stages of degeneration [7]. However, challenges such as activation of RGCs axon bundles have limited the spatial resolution of epiretinal prostheses [8]. In fact, some subjects with epiretinal implants have reported the perception of elongated phosphenes due to electrical stimulation [9].

Research has been conducted on the direct stimulation of RGCs using short pulse durations to improve the effectiveness of current epiretinal implants [10–14]. Studies have also investigated indirect activation of RGCs by targeting the presynaptic terminals at the level of bipolar cells (BCs) such that the axonal activation of RGCs can be limited [15–17]. Low frequency sinusoidal electrical stimulation (5–25 Hz) has been shown to indirectly stimulate RGCs [15, 16]. Further, *in-vitro* experiments using the calcium imaging technique and clinical studies have suggested that more focal response of RGCs and round shape of phosphene perception can be achieved using long pulse durations (25 ms) [17].

The sensitivity of BCs response to epiretinal electrical stimulation has been considered in a few studies [18-21]. Margalit and Thoreson have shown that long stimulus pulse durations mediate neurotransmitter release at the terminals of BCs [18]. Recently, a photoreceptor peeling method has been utilized to directly record the response of BCs to epiretinal stimulation of various stimulus amplitude and long pulse durations in the wholemount retina [20]. The ON-type BCs have shown to be more sensitive to long pulse widths and no significant difference has been observed between the healthy and degenerated (rd10 mice) [21]. Most recently, a biophysically realistic model of ON-BCs has been developed comparing the modeling results with the experimentally recorded response of BCs to epiretinal electrical stimulation [22].

Despite these successes, the mechanisms underlying selective excitation of BCs and the networkmediated response of RGCs with long stimulus pulse widths are not well understood. The contribution of T-type and L-type of calcium (Ca) channels at the terminal of BCs to the great sensitivity of BCs to low-frequency stimulation has been studied [19]. The slow kinetics of calcium channels has been suggested as a possible underlying mechanism for the high sensitivity of BCs to low stimulation frequencies. Although both T-type and L-type Ca channels can play roles in regulating neurotransmitter release at the terminals of BCs, the impact of hyperpolarizationactivated cyclic nucleotide-gated (HCN) channels on modulating the membrane potential at the BCs synaptic terminals has not been investigated. A high concentration of HCN channels has been expressed at the terminals of BCs and photoreceptors [23, 24]. Therefore, a better understanding of the influence of HCN channels on the BCs response to electrical stimulation would allow us to gain additional insights into

the sensitivity of BCs to a range of stimulus pulse durations.

The direct stimulation threshold of A2-RGCs has been reported to be the lowest using asymmetric short cathodic-first biphasic pulses [25]. However, reduced stimulation thresholds of RGCs and perceptual threshold of subjects with epiretinal implants stimulated with asymmetric long anodic-first pulses has been recently shown [11, 26]. The anodic break excitation mechanism has been shown to play a role in decreasing the threshold of cells using long anodic-first pulses [25, 27]. However, the impact of asymmetric stimulus pulses on the response of BCs and therefore indirect activation of RGCs is still unknown.

In this work, we utilized our computational modeling platform, AM/NEURON [28-37], to better understand the response of retinal BCs to electrical stimulation as a function of various stimulation parameters. This modeling platform will enable us to capture factors affecting the responsiveness of BCs through alterations of the electrical stimulation waveforms. To this aim, we implemented computational models of BCs of the primate retina that are known to generate action potentials. Recently, the detailed model of spiking BCs incorporating the accurate distribution of ion channel densities has been implemented [38, 39]. These spiking BCs in the magnocellular pathway are capable of generating strong synaptic activities at their axonal terminals leading to a greater likelihood for indirection activation of RGCs. Therefore, this BC subtype is a good candidate for evaluating the stimulation threshold and response of the cell to a range of stimulus parameters. This sensitivity analysis ultimately allows us to determine the stimulation strategies leading to the reduced stimulation threshold of BCs and therefore the higher chance for indirect activation of RGCs.

Utilizing this model, we first investigated the BCs response characteristics to epiretinal electrical stimulation of various monophasic and biphasic symmetric charge-balanced stimulus pulses. We determined the correlations of amplitude, pulse duration, membrane potential, and response latency of BCs. The impact of the HCN ion kinetics on the sensitivity of BCs to modulations in pulse durations and stimulus waveforms was examined. Our results show that the membrane voltage is significantly affected by alterations in pulse width and current amplitude. The hyperpolarization before the depolarization of the membrane notably influences the stimulus threshold of BCs over a range of pulse durations. Anodicfirst symmetric biphasic waveforms with long stimulus pulse widths are found to better reduce the stimulation threshold of BCs compared to that of cathodic-first biphasic pulses, thereby suggesting the greater potential for mediating synaptic release at the pre-synaptic terminals using a lower stimulus amplitude.

We further investigated the influence of the waveform asymmetry on the stimulus threshold of BCs. The findings of our computational modeling study and correlations with the experimental data from the literature will help us utilize this modeling platform for designing stimulus waveforms and improving the effectiveness of current retinal prosthetic systems.

2. Methods

2.1. Admittance method (AM)/NEURON computational framework

Our multi-scale computational framework utilizes three-dimensional (3D) AM and NEURON simulations to model electrical stimulation of retinal tissue and simulates the responses of retinal neurons [28–37]. First, AM is used to compute the voltage distribution inside the extracellular space. Then, this voltage distribution is applied to the multicompartmental models of neurons to measure spatiotemporal activities using NEURON simulations.

2.2. Admittance method (AM): constructing the retina tissue and electrodes

The AM-NEURON platform divides the modeling of electrical stimulation of neural tissues into two steps. First, the AM is used to model the 3D bulk neural tissue and estimate the stimulation-induced voltages at all locations of the tissue. Next, Neuron software is used to model the biophysical behavior of the neurons accurately; the interpolated AM computed voltages are applied as the extracellular voltages at various sectional of the neurons, and neural responses are simulated.

To create the bulk tissue model, we constructed a 3D computational model of a section of the retinal tissue and implant electronics. This model consists of various retinal layers with appropriate thickness, stimulating electrodes, and the ground electrode. The model is discretized using non-uniform mesh to reduce the computation time while ensuring the accuracy of simulation results. The AM discretizes the model in more than 18 million computational cells, and each cell is represented by the admittance values of corresponding material at its edges. AM has advantages in modeling of electrical stimulation of neural tissue compared to other numerical methods, as it represents the 3D bulk tissue model using a network of admittances; and thus, provides a simplified way to add arbitrary electric components to model bioelectromagnetics elements, such as tissueelectrode interfaces [28]. The AM considers the stimulating electrode currents as the source and solves the admittance network with the help of numerical methods, such as the bi-conjugate gradient method, to estimate the induced voltages at every node of the tissue model.

In our retinal tissue model, we have modified the thickness and structure of retinal layers to mimic the structural changes observed in the degenerated retinal tissue. The dielectric properties of the retina and electronic components are based on our previous work [33, 35]. A stimulating electrode of a diameter of 200 μ m is placed on the top-center of the bulk retina tissue and is positioned 50 μ m from the presynaptic terminals of computational models of the BCs. Stimulus current is applied to a single electrode and the resulting voltages are calculated at each node of the bulk tissue model using AM. A linear interpolation function was used to estimate the voltages at the center of each neuronal compartment using node voltages; these interpolated values are then applied as extracellular voltages in NEURON simulations. Further details about the computational framework can be found in [28-37]. The AM-NEURON computational platform has been recently parallelized by our group and accommodates adaptive multiresolution meshing. In this work, the dimensions of the constructed discrete model are the same as our previous work [12] with $300 \times 300 \times 200$ voxels and the minimum model spatial resolution was set to 10 μ m and in regions of lower resolution at most 64 voxels were merged. To perform different types of analysis in this work, we have considered monophasic, symmetric biphasic, and asymmetric biphasic charge-balanced pulses of varying pulse durations ranging from 0.1 to 100 ms with no interphase gap (IPG) in this study.

2.3. NEURON: BCs modeling

To model the spiking BCs, we first extracted the morphology as an SWC file from [39] and imported it into NEURON software as shown in figure 1(a). This multi-compartmental model is finely compartmentalized with non-uniform distribution of ionic channels at each section and their response characteristics to a range of electrical stimulation parameters are investigated. The resulting DB4-BCs compartmental model consists of several ionic currents including the sodium, slow and fast potassium, L-type and Ttype calcium, and hyperpolarization-activated current [40]. The ability of these cells to generate spikes represents a strong release of neurotransmitters at the terminal of BCs and a quicker signals transformation from the photoreceptor to RGCs. The modeling of this type of BCs enabled us to determine the stimulation threshold of this cell to the electrical stimulation of various stimulus parameters. The stimulation threshold is defined as the minimum current to generate an action potential in the cell during the cathodic stimulation phase. The expressions for most of the ionic currents including the gating variables and rate constants for different sections (soma, dendrites, axon, terminal) are similar to [39]. The L-type calcium channel has been adjusted from the previous study and the ionic kinetics are provided by [40]:

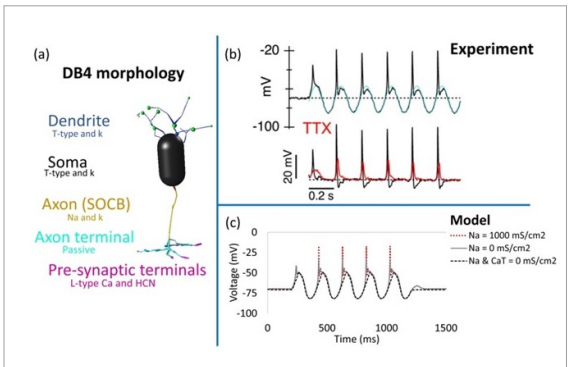


Figure 1. The verification of the developed model of spiking BCs in response to intracellular stimulation. (a) The morphology of the DB4 BC; (b) experimental data from [42] showing the response of the cell to a sinusoidal current of 10 pA in amplitude at the frequency of 20 Hz; (c) the response of our multi-compartment model of the DB4 cell to the sinusoidal input current. The model can closely replicate the experimentally recorded signal and the characteristics of sodium and calcium spikes have been further shown in the figure.

Table 1. Maximum ionic conductance values (ms cm^{-2}).

	Soma	Dendrite	Axon	Presynaptic terminal	Terminal
g _{Na}	_	_	1000	_	_
g_{Kslow}	0.6	2.4	_	_	_
g_{Kfast}		_	2	_	_
g_{caL}		_		1	_
g_{caT}	1	1		_	_
g _{HCN}		_		3.25	_
g_1	0.033	0.033	0.033	0.033	0.033

$$i_{\text{CaL}} = g_{\text{caL}}c^{3}(V - E_{\text{caL}})$$

$$\frac{dc}{dt} = -(\alpha_{c} + \beta_{c})c + \alpha_{c}$$

$$\alpha_{c} = \frac{-0.3(V + 70)}{e^{-0.1}(V + 70) - 1}$$

$$\beta_{c} = 10e^{-(V + 38)/9}$$

where g_{CaL} is the maximum ionic conductance of the L-type calcium and *c* is the activation gating variable. α and β are rate constants for the opening and closing of the ionic channels. The reversal potential of the calcium channel (E_{caL}) was calculated based on the intracellular concentration of the calcium and is similar to Fohlmeister et al [41]. The extracellular calcium concentration is set to 1.8 mM. The depth of the calcium pump and the time constant of the calcium current are 0.1 μ m and 1.5 ms, respectively. The membrane capacitance is set to 1 μ F cm⁻² and 100 Ω cm is selected for the intracellular resistivity. The maximum ionic conductance values of each section of this BC subtype are provided in table 1. Further details of the remaining parameters and variables can be found in [39].

3. Results

3.1. Intracellular stimulation: NEURON simulation

To validate the modeled DB4-BC subtype, we compared the response of the cell to intracellular stimulation with the experimentally recorded signals of the same spiking BC types [42]. A sinusoidal current of 10 pA amplitude at the stimulation frequency of 20 Hz was injected into the cell and the membrane potential was recorded from the cell body. As illustrated in figures 1(b) and (c), the DB4-BC model can closely predict the experimentally recorded cells, including the initial spikes after the onset of the depolarizing cycle. Similarly to the experiment, both sodium and calcium spikes have been predicted by computational modeling (figure 1(c)). The absence of the Na current decreases the peak value of the depolarizing membrane potential. This result correlates with the electrophysically recorded signals from DB4 cells in the presence of the Na channel blocker, tetrodotoxin (TTX) [42].

Our modeling has further shown the contribution of the T-type calcium channel to the small depolarizing voltage transient measured after the blockage of the voltage-gated Na channels. Setting the densities of Na and Ca-T channels to zero has eliminated the robust spiking in DB4 BCs as shown in figure 1(c).

3.2. Extracellular stimulation: AM/NEURON modeling

We aimed at better understanding the response characteristics of BCs to extracellular stimulation of various parameters. Our computational modeling enabled us to capture the mechanisms for activation of BCs and determine the sensitivity of BCs to electrical stimulation of different pulse durations and waveforms. The cathodic monophasic stimulus pulses with durations ranging from 0.1 to 25 ms were applied and the response of BCs was investigated (figure 2(a)). We applied the minimum current amplitude required to generate an action potential in the cell body for varying stimulus pulse durations. This type of BC generates action potentials with different latencies as the pulse duration changes. At the onset of the cathodic pulse, the membrane voltage at the soma experiences a hyperpolarization with varying durations as the pulse width is altered. These hyperpolarization events arise from the longer distance of the soma from the stimulating electrode relative to the terminals of BCs [38]. Therefore, with a certain delay, the signals backpropagate from the site of spike initiation, axon with the high density of sodium channels, to the soma, leading to the depolarization events at the soma as shown in figure 2(a). Figure 2(b) represents the soma spike latency as a function of alterations in pulse duration. The latency is defined as the time

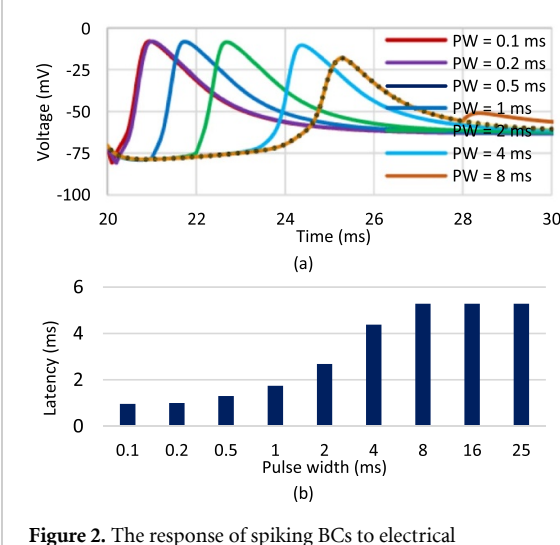


Figure 2. The response of spiking BCs to electrical stimulation of various cathodic-first monophasic pulse durations using AM-NEURON modeling framework.
(a) The simulated membrane potentials as a function of time for pulse widths (PWs) ranging from 0.1 to 25 ms.
(b) Response latency as a function of variations in pulse durations. Results indicate the sensitivity of BCs response to changes in pulse durations.

duration from the onset of the stimulation pulse to the peak of the membrane potential. The latency of the evoked action potential increases as we increase the stimulus pulse duration.

The role of current amplitude modulations in the response latency changes of BCs was considered as shown in figure 3(a). For a given pulse duration of 8 ms, a rapid exponential decrease in the response latency of the cell has been shown as the current amplitude increases. The latency-amplitude curve flattens out around 130 μ A current amplitude having latencies of around 1.1 ms. This indicates the significant contribution of current amplitude in the response delay of BCs to electrical stimulation. Figure 3(b) further shows the membrane potentials of BCs for a range of current amplitude. There is an upper limit for the peak membrane voltage as modulations in current amplitude. Peak membrane voltage is relatively higher for the intermediate current amplitude values. While the low current amplitude and relatively long response latency lead to a slight reduction in the peak membrane potential, large current amplitudes with short spike latency result in a noticeably lower membrane voltage peak at the soma. Therefore, the contribution of current amplitude and pulse duration to the modulations in response latency of BCs to electrical stimulation may ultimately alter the amount of neurotransmitter release at the presynaptic terminals of BCs and thereby the response of the downstream

We further analyzed the stimulus thresholds of BCs for a range of pulse durations from 0.1 to 100 ms in response to a single stimulus pulse of cathodic monophasic, cathodic-first, and anodic-first biphasic pulses (figure 4). We also included the cathodic

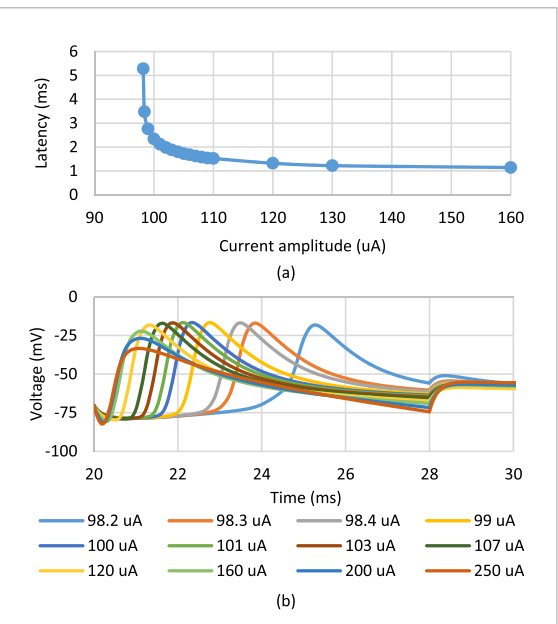


Figure 3. Modulations in the response of BCs a function of changes in current amplitude using cathodic-first monophasic pulse durations. (a) The response latency of BCs as a function of modulations in current amplitude. (b) The time course of the membrane voltage for a range of current amplitudes. Data show the significant impact of current amplitude on the response latency and the membrane potential peak.

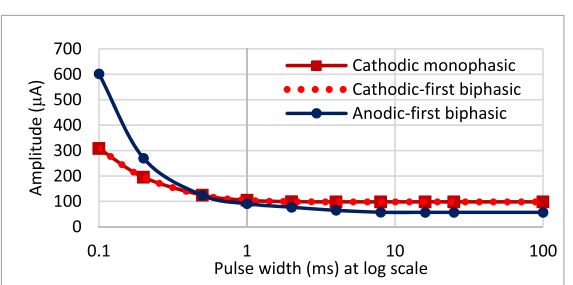


Figure 4. Stimulation strength-duration curve of BCs for cathodic monophasic, cathodic-first and anodic-first biphasic pulses. Our data show that stimulation amplitudes are higher for anodic-first biphasic with shorter stimulus pulse durations. However, the presence of the anodic phase prior to the cathode significantly reduces the threshold of BCs for longer pulse durations. The chronaxie and rheobase of the anodic-first biphasic pulses are 0.6 ms and 57 μ A, respectively. However, the chronaxie and rheobase of the cathodic-first biphasic pulses are 0.2 ms and 98.2 μ A, respectively.

monophasic pulses to isolate and demonstrate the role of the anodic phase in the responsiveness of BCs to various electrical stimulus pulses. Figure 4 shows the stimulus threshold as a function of pulse duration for these stimulus waveforms. Larger current amplitudes are required to reach the threshold for the cathodic monophasic and cathodic-first biphasic pulses with pulse widths less than 0.5 ms. No difference in the stimulus thresholds of BCs was observed using the cathodic monophasic and cathodic-first biphasic pulses. This is due to the occurrence of depolarization events and the opening of sodium gated ion channels during the cathodic phase of

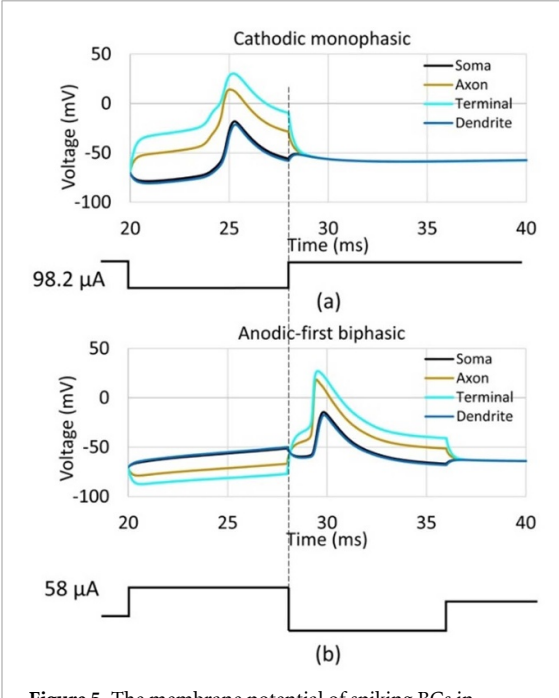


Figure 5. The membrane potential of spiking BCs in response to electrical stimulation of both cathodic monophasic (top) and symmetric anodic-first biphasic (bottom) using a pulse width of PW = 8 ms.

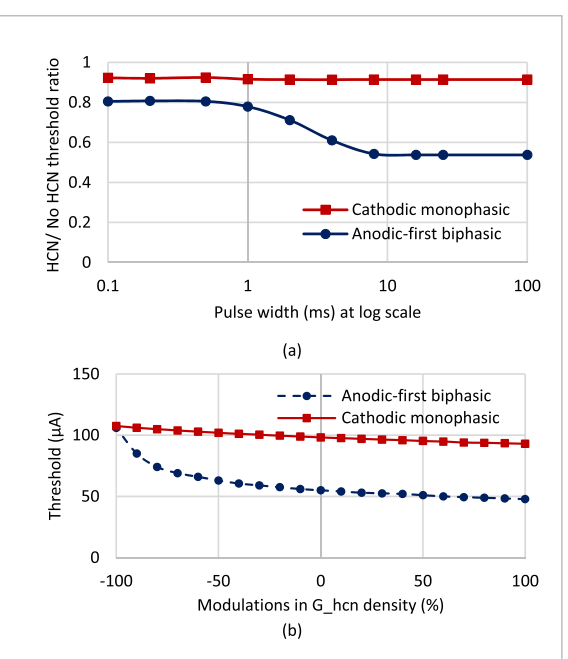


Figure 6. The role of the HCN channels in response of BCs to electrical stimulation. (a) Stimulation BCs threshold difference between simulations with and without the expression of HCN channels. (b) The impact of HCN density on the response of BCs.

stimulation. Interestingly, the longer anodic-first pulses remarkably decrease the stimulation threshold of BCs. The simulation results indicate the role of hyperpolarization events before the depolarization in the reduction of BCs excitation threshold to long stimulus pulses.

Figure 5 shows the response of BCs to electrical stimulation of 8 ms pulse duration for cathodic monophasic and anodic-first biphasic waveforms, as a function of time. Extracellular stimulation of cathodic pulses leads to depolarization of regions close to stimulating electrodes and hyperpolarization of compartments away from electrodes at the onset of stimulation. Therefore, as depicted in figure 5(a) the onset of the cathodic pulse results in the hyperpolarization of soma and dendrites and depolarization of axon and axon terminals. With the opening of sodium channels at the axon initial segment (AIS), the signals backpropagate to the soma and dendrites, leading to the generation of action potentials at the soma and dendrites with a certain latency. During the anodic phase of stimulation, the membrane potential of soma increases over time (figure 5(b)). This change in the potential leads to the increase in the membrane voltage at the onset of the cathodic phase of the stimulation and therefore a reduced stimulation current amplitude is required for spike generations of BCs (as shown in figure 5).

3.3. Role of hyperpolarization activated current (HCN)

To examine the factors influencing the low stimulus threshold of BCs to long anodic-first biphasic pulse durations, we studied the contribution of the HCN channels at the presynaptic terminals to this sensitivity difference. We compared the response of BCs in the presence and absence of HCN channels at the presynaptic terminals for a range of stimulus pulse durations. Figure 6 shows the ratio of BCs stimulus threshold with and without HCN channels expressions for both cathodic monophasic and anodic-first biphasic waveforms. HCN channels have a negligible contribution to the response of BCs to electrical stimulation of different pulse widths for cathodic monophasic pulses (figure 6(a)). This is expected as the HCN channels are closed at the terminals during the depolarization and there is no hyperpolarization at the terminal of the cell with the cathodic monophaisc pulse (figure 5(a)). However, HCN currents are sensitive to anodic-first biphasic pulse modulations due to the initial hyperpolarization at the presynaptic terminals (figure 5(b)). The BCs threshold has been significantly reduced with the addition of HCNs for anodic-first biphasic pulses with pulse widths longer than 8 ms. This indicates the role of HCN currents in the reduction of BCs threshold required for spikes using long anodic-first biphasic pulses.

Different densities of the HCN channels were analyzed to consider the impact of the HCN concentration difference at the terminals on the stimulation threshold of BCs for a given pulse width of 8 ms as demonstrated in figure 6(b). The cathodic monophasic pulses do not have a significant impact on the threshold for a change in the HCN channel densities. However, for the anodic-first biphasic pulses,

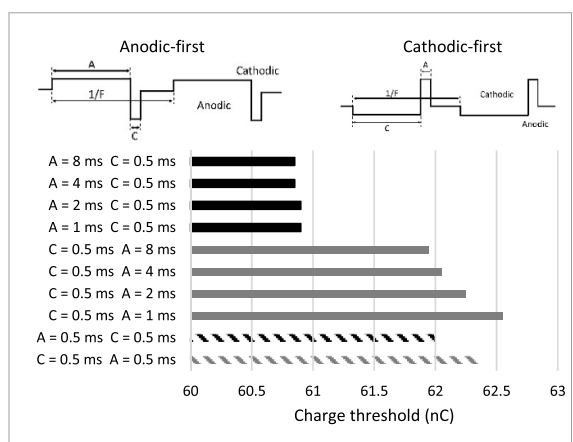


Figure 7. The impact of the asymmetric biphasic pulses on the charge threshold of DB4-BCs. The cathodic pulse duration is set to 0.5 ms and the anodic pulse duration is modulated from 0.5 to 8 ms. The asymmetric anodic-first stimulation has been shown to reduce the BCs charge threshold compared to the anodic-first symmetric, cathodic-first symmetric, and asymmetric cathodic-first biphasic waveforms.

reducing the expression of HCN concentration at the terminals exponentially increases the BCs threshold (figure 6(b)).

3.4. The influence of waveform asymmetry

We further utilized our modeling framework to investigate the effect of asymmetric waveforms on the response of BCs. Due to the asymmetry of chargebalanced stimulus pulses and therefore amplitude and pulse width difference between each phase, we used charge threshold ($Q = I \times PW$) for this investigation. We compared the charge threshold of the cell using asymmetric cathodic-first and anodic-first biphasic pulses to symmetric cathodic-first and anodic-first biphasic stimulations (figure 7). All considered symmetric and asymmetric pulses are charge-balanced. The cathodic pulse duration was constant and equal to 0.5 ms and the anodic pulse duration was altered. Our computational results show that the asymmetric long anodic stimulus pulses lead to the lowest charge threshold of BCs. Therefore, this further indicates the role of membrane potential hyperpolarization in the enhanced sensitivity of the following cathodic phase stimulation. Similar to the results from the previous section (figure 6), the HCN channels at the terminals of BCs can contribute to the low excitation threshold of BCs using asymmetric long anodic-first stimulation pulses.

4. Discussion

In this work, we have utilized our 3D multi-scale AM/NEURON computational modeling framework to gain insights about parameters affecting the response of spiking BCs to electrical stimulation. The impact of pulse duration and amplitude modulations on the response of BCs including the depolarizing membrane potential and the response latency

has been investigated. An increase in current amplitude has been shown to reduce the spike latency of BCs. While the increase of pulse width significantly increases the response latency of the cell at the suprathreshold current (figure 2), an increase in the stimulus amplitude can decrease the spike latency and the timing associated with the opening of the sodium channel gate (figure 3(a)). Our computational findings correlate with the experimental results on the response of ON BCs to epiretinal electrical stimulation using a patch-clamp technique [21]. Our modeling also predicts the reduced peak membrane potential with the huge increase in the stimulus current (figure 3(b)).

Using this platform, we further investigated the response of BCs to different electrical stimulation parameters to find the stimulus waveform design leading to the lowest stimulus threshold of the cell. We found that long anodic-first biphasic stimulations can significantly reduce the stimulus threshold of the DB4 cell. The negative membrane potential at the terminal and axon before the onset of the cathodic stimulation can reduce the inactivation probability of the sodium channels and, therefore, increase the sensitivity of the BCs for the spike initiation. The role of the presence of the HCN channels is significant in decreasing the stimulus threshold of the cell. In the presence of short stimulus pulses, we demonstrated that among various stimulus waveforms designs, the lowest threshold is achieved using an asymmetric long anodic-first biphasic stimulation.

4.1. Computational modeling of DB4-BCs

Previously, it was thought that retinal BCs are passive and provide graded response only. However, later, electrophysiological studies revealed the presence of voltage-gated ionic channels in different types of BCs [24]. Rat cone BCs have been shown to express sodium, calcium, and outward potassium currents [43]. Recent patch-clamp recordings from the ONtype BCs in the wholemount mouse retina further supports the presence of strong outward rectifying potassium currents. The high concentrations of HCN channels have been reported not only in BCs of the magnocellular pathway (DB3 and DB4) of the primate retina but also in photoreceptors and BCs terminals of the rat retina [23]. The DB4-BC model implemented in the present study incorporating different distribution and densities of ionic channels is based on the previously published paper [39]. The Na channels have been shown to enhance the synaptic release at the presynaptic terminals of BCs and excitatory input to parasol RGCs [42], thereby increasing the potential for indirect activation of RGCs. Therefore, we centered our focus on this particular cell type with the high-density Na channels in the AIS.

4.2. Sensitivity of BCs response to electrical stimulation

Studies have shown that select excitation of BCs and, therefore, the network-mediated response of RGCs can be achieved with a low stimulation frequency [16] and long pulse durations [17]. L-type and T-type calcium channels are known to mediate the neurotransmitter release at the presynaptic terminals of BCs. The sensitivity of these calcium channels to electrical stimulation of various frequencies has been conducted in [19]. Furthermore, the response of DB4 spiking BCs to the intracellular and extracellular stimulation of monophasic stimulus pulses has been investigated by Rattay et al [38, 39]. Here, we compared the response of the same type of BCs to epiretinal electrical stimulation incorporating various stimulus waveforms using the disk electrode of the Argus II prosthetic systems [9]. There has been no study specifically focusing on the contribution of HCN channels to the response of BCs to electrical stimulation. We found that the expression of HCN channels at the presynaptic terminals of BCs remarkably influences the reduced reduction in the threshold of the cell using long anodic-first stimulus pulses (figure 6). We found that the absence of HCN channels at the presynaptic terminals of BCs increases the stimulus threshold of BCs. Therefore, in addition to the slow kinetics of calcium channels [19], HCN channels also contribute to the higher sensitivity of BCs to long biphasic stimulus pulse and low-frequency stimulation. Notably, the presence of the HCN current during the hyperpolarizing phase of the sinusoidal intracellular stimulation and the role of HCN current in spike generation of the cell during the depolarizing phase have been also demonstrated in both modeling and experimental results [39, 42]. Interestingly, high contrast light stimulus inputs have been shown to contribute to the great negative fluctuation in membrane potential. The negative phase of the membrane potential can therefore activate HCN channels, augmenting the potential for BCs spike generation following negative fluctuations during positive cycles [42, 44]. Therefore, understanding the contribution of the HCN channels to BCs response allows us to better design epiretinal electrical stimulus parameters, increase the likelihood for the indirect activation of RGCs and, therefore, help avoid the excitation of RGCs axon bundles.

Our computational findings can be further extended to other types of retinal prosthetic devices such as subretinal and photovoltaic implants. The major difference between epiretinal and subretinal prostheses is the placement of the stimulating electrode array. Therefore, placing the stimulating electrode close to dendrites of BCs compared to terminals of cells would mostly change the polarity of stimulus waveforms [38]. Therefore, symmetric cathodic-first biphasic pulses with long pulse durations, and not long anodic-first biphasic stimulus pulses, can

decrease the stimulation threshold of BCs in response to subretinal electrical stimulation.

The sensitivity of direct and network-mediated response of RGCs to epi, sub-, and intraretinal electrical stimulation with varying monophasic cathodic and anodic pulse widths has been investigated [45]. The authors found that the indirect stimulation thresholds of RGCs in response to subretinal stimulation were lower using anodic pulses compared to cathodic pulses, therefore anodic stimulus pulses have been used in clinical studies [46]. However, the experimental study only focused on monophasic stimulus pulses and the impact of anodicfirst and biphasic pulses on the network-mediated response of RGCs was not investigated. While it has been well established that anodic monophasic pulses lead to the lower stimulation threshold of BCs relative to cathodic monophasic pulses in the case of subretinal electrical stimulations, the cathodic phase of the cathodic-first biphasic pulse can augment the probability BCs spiking during the anodic stimulation phase. The influence of cathodicfirst biphasic pulses on perceptual thresholds of patients with subretinal implants remains to be investigated.

4.3. Asymmetric electrical stimulation of retinal neurons

Epiretinal electrical stimulation of the A2-type RGCs using asymmetric cathodic-first biphasic waveforms with short cathodic pulses has been reported to increase the efficacy of stimulation [25]. A recent experiment using a calcium imaging technique has reported the lowest threshold of RGCs using asymmetric long anodic-first stimulus pulses [11]. Therefore, we investigated these two asymmetric waveforms in addition to both symmetric cathodic and anodic-first biphasic stimulations (figure 7). This analysis allowed us to better understand the contribution of the network-mediated response of RGCs to electrical stimulation.

The reduction of the Na inactivation probability during the hyperpolarization phase has been shown to play a role in the reduced threshold of cells. Electrical stimulation of nerve fibers with long anodic-first biphasic waveforms resulted in a high chance of spike generation at the onset of the cathodic stimulation [27]. The response of the RGCs model to electrical stimulation indicated that the lowest stimulus threshold of the cell can be achieved using an asymmetric long anodic-first stimulation with the addition of an IPG [26]. However, the direct stimulation threshold of RGCs in the absence of the IPG is the lowest using the asymmetric short cathodic-first waveforms [25]. Therefore, analyzing the response of the isolated RGCs may not fully explain the calcium imaging experimental observations of the lowest threshold of the stimulated retinal network using asymmetric long anodic-first

waveforms with no IPG. In the present study, we have shown the greater sensitivity of BCs to the asymmetric long anodic-first stimulation compared to both short symmetric (cathodic- and anodic-first) and asymmetric cathodic-first biphasic stimulations (figure 7). This indicates the high likelihood of neurotransmitters release and excitatory inputs to RGCs, suggesting the reduced indirect stimulation threshold of RGCs. The computational findings of this study may explain the role of the network-mediated response of RGCs as well as the presence of HCN channels at the terminals of BCs in higher stimulation efficacy of asymmetric long anodic-first pulses.

4.4. Clinical implications

Clinical testing with epiretinal implant subjects has proven the efficacy of long biphasic pulses and low stimulation frequencies for improving the spatial resolution of these devices [17]. In this study, we have explored the role of an anodic phase following by a cathodic phase in the reduction of stimulation threshold at the presynaptic terminals of BCs using long pulse durations. This indicates the likelihood to avoid activation of RGCs axon bundles and indirect excitation of RGCs. At a low biphasic stimulation frequency of 20 Hz and 25 ms pulse width utilized in the subject testing, every cathodic phase is followed by an anodic phase. Therefore, the presence of the hyperpolarizing event prior to the depolarization as well as the high concentration of the HCN channels at terminals of both photoreceptors and BCs may reduce the threshold necessary for indirect activation of RGCs, thereby avoiding axonal activation of RGCs and better outcome of current epiretinal prosthetic systems. This computational platform allowed us to propose a potential indirect activation strategy for a more focal response of RGCs using long pulses.

Recent clinical testing with three Argus II subjects has revealed the reduced perceptual threshold (on average) and great percept brightness of asymmetric long anodic-first stimulation [26]. Our computational findings correlate with the clinical results, suggesting the plausible contribution of the network-mediated response of RGCs in the reduced perceptual threshold of these subjects. This supports the potential of our multi-scale predictive modeling framework, which allows us to better capture factors influencing the response of retinal neurons to electrical stimulation and ultimately design stimulation strategies for enhancing the effectiveness of prosthetic devices.

This modeling framework and the response of retinal neurons to epiretinal electrical stimulation can be extended to other therapeutic techniques. For instance, the application of transcorneal electrical stimulation (TES) for slowing down the progression of retinal blindness in RP and AMD patients. The influence of TES on the reduced progressive loss of

visual field area in RP patients using symmetric long anodic-first biphasic pulses has been demonstrated in the clinic [47, 48]. This may further support our findings that long anodic-first pulses can reduce the stimulation threshold of BCs that are affected first along with photoreceptors at the early stage of retinal degeneration and potentially opening avenues to slow down the progression of retinal blindness.

4.5. Current amplitudes and neural tissue safety

The range of computed stimulus threshold amplitudes in the present study is similar to clinical studies with Argus I and Argus II subjects [49, 50]. It has also been shown that perceptual thresholds of subjects with epiretinal implants can increase to more than 250 μ A 43 months post-surgery [50]. To look at the tissue damage aspects, we performed a safety analysis for the considered stimulation waveforms, as in our previous work of waveform design [35]. According to Shannon's equation and McCreery's tissue safety criteria based on charge and charge density, the damage is observed for $k \ge 1.85$ [51, 52]. Here, k is defined by the equation $k = \log(Q) + \log(D)$, where Q is the charge per phase and D is the charge density per phase. A 200 μ m diameter electrode stimulated with a current amplitude of 100 μ A and a pulse duration of 0.5 ms leads to the charge current density of 159 μ C cm² ph⁻¹ and the charge of 0.05 μ C ph⁻¹. Therefore, for the waveforms and electrode size considered in this work, the value of k (0.9) is well within the safety limit. The differences in the range of stimulation thresholds of BCs reported in the present work and other modeling and experimental studies from the literature [21, 38, 53] arises from factors such as electrode size, location of electrode across retinal lavers, and retinal tissue resistivity based on the stage of degeneration.

4.6. Limitations and future work

This study is limited to BCs in the magnocellular pathway with a high density of the sodium channels in the AIS. While there have been subtypes of BCs in mouse and rat retinas with the expression of Na [43, 54], there are many ON and OFF BCs that do not express Na channels and their response to electrical stimulation needs to be analyzed. The impact of fibrous tissue growth under the electrode array that modulates the impedance and therefore perceptual threshold of retinal prosthetic devices was not considered in this study. Further, we only considered the response of BCs to electrical stimulation for a fixed electrode position and electrode-cell distance. Modeling a large population of BCs and computing the 2D stimulation threshold map in the retina would provide a more realistic computational model for understanding the BCs response to electrical stimulation. In the future, we will incorporate other BCs subtypes as well as the realistic network of the retina to better capture the response of the retinal neurons to external stimulation and improve the performance of current epiretinal prosthetic systems. Our group is working on connectome-based retinal network modeling of various stages of retinal degeneration [55, 56]. These models will help us understand the changes in the retinal network with the progression of the disease and potentially help in designing better stimulation strategies.

To the best of our knowledge, no electrophysiological studies have been conducted so far focusing on the influence of HCN channels on the response of BCs to electrical stimulation. Therefore, future experiments can further explore the role of this channel in the sensitivity of different BCs subtypes to various electrical stimulation parameters. Recently, the weakened network-mediated response of RGCs to epiretinal electrical stimulation at the late stage of degeneration has been reported [57, 58]. This outlines the importance of this study and designing electrical stimulus parameters for reducing the threshold of outer retinal neurons and thereby improving the outcome of retinal implants.

5. Conclusion

Using our 3D multi-scale AM/NEURON computational modeling framework, we have implemented the spiking BCs model and predicted its response under epiretinal electrical stimulation. We validated our model against available computational models and experimental data from the literature. We investigated the response of BCs to different monophasic, symmetric, and asymmetric biphasic stimulus waveform designs with various current amplitudes and pulse widths. We found that the stimulation threshold of BCs was reduced using symmetric long anodicfirst biphasic pulses compared to long cathodicfirst biphasic pulses. We further explored the role of HCN channels at the presynaptic terminals in the reduced stimulus threshold observed using long pulses with anodic-first phases. Further, the stimulation threshold of BCs with asymmetric long anodicfirst pulses was found to be lower relative to that of asymmetric short cathodic-first pulses. This computational platform allowed us to gain a deeper understanding of the mechanisms underlying the excitation of retinal neurons to different stimulation waveforms and find potential answers to missing puzzles of animal and clinical studies from the literature. Our predictive modeling framework will further help design and test the stimulation strategies to enhance the effectiveness of retinal prosthetic systems.

Data availability statement

The data that support the findings of this study are available upon reasonable request from the authors.

Acknowledgments

This work was supported by the EFRI NSF (Award No. 1933394), NEI (NIH Grant No. R21EY028744), the NIBIB (NIH Grant No. U01EB025830), and an unrestricted grant to the Department of Ophthalmology from Research to Prevent Blindness, New York, NY

ORCID iDs

Javad Paknahad https://orcid.org/0000-0003-3315-3495

Pragya Kosta https://orcid.org/0000-0002-2141-8700

Jean-Marie C Bouteiller https://orcid.org/0000-0003-3069-0826

References

- [1] Humayun M S, de Juan E Jr, Weiland J D, Dagnelie G, Katona S and Greenberg R *et al* 1999 Pattern electrical stimulation of the human retina *Vis. Res.* **39** 2569–76
- [2] Humayun M S, Weiland J D, Chader G and Greenbaum E 2007 Artificial Sight Basic Research, Biomedical Engineering, and Clinical Advances 1st edn (New York: Springer)
- [3] Weiland J D and Humayun M S 2014 Retinal prosthesis TBME 61 1412–24
- [4] Weiland J D, Walston S T and Humayun M S 2016 Electrical stimulation of the retina to produce artificial vision Annu. Rev. Vis. Sci. 2 273–94
- [5] Zrenner E et al 2011 Subretinal electronic chips allow blind patients to read letters and combine them to words Proc. R. Soc. B 278 1489–97
- [6] Kosta P et al 2018 Electromagnetic safety assessment of a cortical implant for vision restoration IEEE J. Electromagn. RF Microw. Med. Biol. 2 56–63
- [7] Marc R E, Jones B W, Watt C B and Strettoi E 2003 Neural remodeling in retinal degeneration *Prog. Retin. Eye Res.* 22 607–55
- [8] Nanduri D et al 2012 Frequency and amplitude modulation have different effects on the percepts elicited by retinal stimulation Invest. Ophthalmol. Vis. Sci. 53 205–14
- [9] Beyeler M, Nanduri D, Weiland J D, Rokem A, Boynton G M and Fine I 2019 A model of ganglion axon pathways accounts for percepts elicited by retinal implants Sci. Rep. 9 9199–16
- [10] Jensen R J, Ziv O R and Rizzo J F 2005 Thresholds for activation of rabbit retinal ganglion cells with relatively large, extracellular microelectrodes *Invest. Ophthalmol. Vis. Sci.* 46 1486 Proceedings. Biological sciences. 2011;278(1711):1489–97
- [11] Chang Y, Ghaffari D H, Chow R H and Weiland J D 2019 Stimulation strategies for selective activation of retinal ganglion cell soma and threshold reduction J. Neural. Eng. 16 026017
- [12] Paknahad J, Loizos K, Humayun M and Lazzi G 2020 Targeted stimulation of retinal ganglion cells in epiretinal prostheses: a multiscale computational study *IEEE Trans. Neural. Syst. Rehabil. Eng.* 28 2548–56
- [13] Jensen R J, Ziv O R and Rizzo J F 2005 Responses of rabbit retinal ganglion cells to electrical stimulation with an epiretinal electrode J. Neural Eng. 2 S16–21
- [14] Fried S I, Hsueh H A and Werblin F S 2006 A method for generating precise temporal patterns of retinal spiking using prosthetic stimulation J. Neurophysiol. 95 970–8
- [15] Freeman D K et al 2010 Selective activation of neuronal targets with sinusoidal electric stimulation J. Neurophysiol. 104 2778–91

- [16] Twyford P and Fried S 2016 The retinal response to sinusoidal electrical stimulation TNSRE 24 413–23
- [17] Weitz A C et al 2015 Improving the spatial resolution of epiretinal implants by increasing stimulus pulse duration Sci. Transl. Med. 7 318ra203
- [18] Margalit E and Thoreson W B 2006 Inner retinal mechanisms engaged by retinal electrical stimulation *Invest*. *Ophthalmol. Vis. Sci.* 47 2606–12
- [19] Freeman D K, Jeng J S, Kelly S K, Hartveit E and Fried S I 2011 Calcium channel dynamics limit synaptic release in response to prosthetic stimulation with sinusoidal waveforms J. Neural. Eng. 8 046005
- [20] Walston S T, Chang Y, Weiland J D and Chow R H 2017 Method to remove photoreceptors from whole mount retina in vitro J. Neurophysiol. 118 2763–9
- [21] Walston S T, Chow R H and Weiland J D 2018 Direct measurement of bipolar cell responses to electrical stimulation in wholemount mouse retina J. Neural Eng. 15 046003
- [22] Paknahad J, Kosta P, Iseri E, Farzad S, Bouteiller J C, Humayun M S and Lazzi G 2021 Modeling ON cone bipolar cells for electrical stimulation Annual Int. Conf. IEEE Engineering in Medicine and Biology Society IEEE Engineering in Medicine and Biology Society. Annual International Conf. (accepted)
- [23] Müller F, Scholten A, Ivanova E, Haverkamp S, Kremmer E and Kaupp U B 2003 HCN channels are expressed differentially in retinal bipolar cells and concentrated at synaptic terminals Eur. J. Neurosci. 17 2084–96
- [24] Benav H 2012 Modeling effects of extracellular stimulation on retinal bipolar cells *Dissertation*
- [25] Hadjinicolaou A E et al 2015 Optimizing the electrical stimulation of retinal ganglion cells TNSRE 23 169–78
- [26] Haji Ghaffari D et al 2020 The effect of waveform asymmetry on perception with epiretinal prostheses J. Neural Eng. 17 45009–045009
- [27] Grill W M and Mortimer J T 1995 Stimulus waveforms for selective neural stimulation EMB-M 14 375–85
- [28] Cela C J A multiresolution admittance method for large-scale bioelectromagnetic interactions 2010 Dissertation North Carolina State University, United States—North Carolina (https://doi.org/10.1109/IEMBS.2010.5628058)
- [29] Paknahad J, Loizos K, Humayun M and Lazzi G 2020 Responsiveness of retinal ganglion cells through frequency modulation of electrical stimulation: a computational modeling study Annual Int. Conf. IEEE Engineering in Medicine and Biology Society vol 2020 pp 3393–8
- [30] Paknahad J, Loizos K, Yue L, Humayun M S and Lazzi G 2021 Color and cellular selectivity of retinal ganglion cell subtypes through frequency modulation of electrical stimulation Sci. Rep. 11 5177
- [31] Paknahad J, Kosta P, Bouteiller J C, Humayun M S and Lazzi G 2021 The sensitivity of retinal bipolar cells response to long stimulus pulse durations in epiretinal prostheses *Invest. Ophthalmol. Vis. Sci.* 62 3169
- [32] Gokoffski K, Paknahad J, Lazzi G and Minimally Invasive A 2021 Approach to electrically stimulating the optic nerve to direct retinal ganglion cell axon regeneration *Invest*. Ophthalmol. Vis. Sci. 62 3013
- [33] Loizos K, Marc R, Humayun M, Anderson J R, Jones B W and Lazzi G 2018 Increasing electrical stimulation efficacy in degenerated retina: stimulus waveform design in a multiscale computational model *IEEE Trans. Neural Syst. Rehabil. Eng.* 26 1111–20
- [34] Stang J et al 2019 Recent advances in computational and experimental bioelectromagnetics for neuroprosthetics ICEAA 1382
- [35] Kosta P, Loizos K and Lazzi G 2020 Stimulus waveform design for decreasing charge and increasing stimulation selectivity in retinal prostheses *Healthc. Technol. Lett.* 7 66–71
- [36] Bingham C S et al 2020 Admittance method for estimating local field potentials generated in a multi-scale neuron model of the hippocampus Front. Comput. Neurosci. 14 72

- [37] Loizos K, RamRakhyani A K, Anderson J, Marc R and Lazzi G 2016 On the computation of a retina resistivity profile for applications in multi-scale modeling of electrical stimulation and absorption *Phys. Med. Biol.* 61 4491–505
- [38] Rattay F, Bassereh H and Fellner A 2017 Impact of electrode position on the elicitation of sodium spikes in retinal bipolar cells Sci. Rep. 7 17590
- [39] Rattay F, Bassereh H and Stiennon I 2018 Compartment models for the electrical stimulation of retinal bipolar cells PLoS One 13 e0209123
- [40] Werginz P and Rattay F 2016 The impact of calcium current reversal on neurotransmitter release in the electrically stimulated retina J. Neural Eng. 13 046013
- [41] Fohlmeister J F and Miller R F 1997 Impulse encoding mechanisms of ganglion cells in the tiger salamander retina J. Neurophysiol. 78 1935–47
- [42] Puthussery T, Venkataramani S, Gayet-Primo J, Smith R G and Taylor W 2013 NaV1.1 channels in axon initial segments of bipolar cells augment input to magnocellular visual pathways in the primate retina *J. Neurosci.* 33 16045–59
- [43] Pan Z H and Hu H J 2000 Voltage-dependent Na⁺ currents in mammalian retinal cone bipolar cells *J. Neurophysiol*. 84 2564–71
- [44] DeVries S H 2000 Bipolar cells use kainate and AMPA receptors to filter visual information into separate channels *Neuron* 28 847–56
- [45] Boinagrov D, Pangratz-Fuehrer S, Goetz G and Palanker D 2014 Selectivity of direct and network-mediated stimulation of the retinal ganglion cells with epi-, sub- and intraretinal electrodes J. Neural Eng. 11 026008
- [46] Palanker D, Le Mer Y, Mohand-Said S, Muqit M and Sahel J A 2020 Photovoltaic restoration of central vision in atrophic age-related macular degeneration *Ophthalmology* 127 1097–104
- [47] Schatz A et al 2011 Transcorneal electrical stimulation for patients with retinitis pigmentosa: a prospective, randomized, sham-controlled exploratory study *Investig.* Ophthalmol. Vis. Sci. 52 4485–96
- [48] Schatz A et al 2017 Transcorneal electrical stimulation for patients with retinitis pigmentosa: a prospective, randomized, sham-controlled follow-up study over 1 year *Investig. Ophthalmol. Vis. Sci.* 58 257–69
- [49] Yue L, Castillo J, Gonzalez A C, Neitz J and Humayun M S 2021 Restoring color perception to the blind: an electrical stimulation strategy of retina in patients with end-stage retinitis pigmentosa *Ophthalmology* 128 453–62
- [50] Yue L, Wuyyuru V, Gonzalez-Calle A, Dorn J D and Humayun M S 2020 Retina-electrode interface properties and vision restoration by two generations of retinal prostheses in one patient-one in each eye J. Neural Eng. 17 026020
- [51] Shannon R V 1992 A model of safe levels for electrical stimulation IEEE Trans. Biomed. Eng. 39 424–6
- [52] McCreery D B, Agnew W F, Yuen T G and Bullara L 1990 Charge density and charge per phase as cofactors in neural injury induced by electrical stimulation *IEEE Trans. Biomed.* Eng. 37 996–1001
- [53] Oesterle J et al 2020 Bayesian inference for biophysical neuron models enables stimulus optimization for retinal neuroprosthetics Elife 9 1–38
- [54] Hellmer C B, Zhou Y, Fyk-Kolodziej B, Hu Z and Ichinose T 2015 Morphological and physiological analysis of type-5 and other bipolar cells in the mouse retina *Neuroscience* 315 246–58
- [55] Pfeiffer R L et al 2020 A pathoconnectome of early neurodegeneration: network changes in retinal degeneration Exp. Eye Res. 199 108196
- [56] Kosta P et al 2021 Model-based comparison of current flow in rod bipolar cells of healthy and early-stage degenerated retina Exp. Eye Res. 207 108554

- [57] Yoon Y J et al 2020 Retinal degeneration reduces consistency of network-mediated responses arising in ganglion cells to electric stimulation IEEE Trans. Neural. Syst. Rehabil. Eng. 28 1921–30
- [58] Corna A, Ramesh P, Jetter F, Lee M, Macke J H and Zeck G 2021 Discrimination of simple objects decoded from the output of retinal ganglion cells upon sinusoidal electrical stimulation J. Neural Eng. 18